POLRADS: polarization radiance distribution measurement system

Kenneth J. Voss,[1,*] and Nordine Souaidia,[1,2]

[1]*Physics Department, University of Miami, 1320 Campo Sano Drive, Coral Gables, Florida, 33146, USA*
[2]*Currently with OPTIS, ZE de La Farlède, BP 275, Toulon, 83278, France*
**voss@physics.miami.edu*

Abstract: While the upwelling radiance distribution in the ocean can be highly polarized, there are few measurements of this parameter in the open ocean. To obtain the polarized in-water upwelling spectral radiance distribution data we have developed the POLRADS instrument. This instrument is based on the NuRADS radiance distribution camera systems in which linear polarizer's have been installed. By combining simultaneous images from three NuRADS instruments, three Stokes parameters (I, Q, U) for the water leaving radiance can be obtained for all upwelling angles simultaneously. This system measures the Stokes parameters *Q/I* and *U/I* with a 0.05-0.06 uncertainty and *I* with a 7-10% uncertainty.

OCIS codes: (010.4450) Ocean Optics; (120.5410) Polarimetry; (010.4458) Oceanic scattering.

References and links

1. T. H. Waterman, "Underwater light and orientation of animals," in *Optical Aspects of Oceanography*, N. G. Jerlov and E. S. Nielsen eds., (Academic Press, New York, NY. 1974).
2. T. W. Cronin, N. Shashar, R. L. Caldwell, J. Marshall, A. G. Cheroske, and T. H. Chiou, "Polarization vision and its role in biological signaling," Integr. Comp. Biol. **43**(4), 549–558 (2003).
3. M. I. Mishchenko, B. Cairns, G. Kopp, C. F. Shueler, B. A. Fafaul, J. E. Hansen, R. J. Hooker, T. Itchkawich, H. B. Maring, and L. D. Travis, "Accurate monitoring of terrestrial aerosols and total solar irradiance: Introducing the Glory Mission," Bull. Am. Meteorol. Soc. **88**(5), 677–691 (2007).
4. H. Loisel, L. Duforet, D. Dessailly, M. Chami, and P. Dubuisson, "Investigation of the variations in the water leaving polarized reflectance from the POLDER satellite data over two biogeochemical contrasted oceanic areas," Opt. Express **16**(17), 12905–12918 (2008).
5. G. Meister, E. J. Kwiatkowska, B. A. Franz, F. S. Patt, G. C. Feldman, and C. R. McClain, "Moderate-resolution imaging spectroradiometer ocean color polarization correction," Appl. Opt. **44**(26), 5524–5535 (2005).
6. K. J. Voss, "Electro-optic camera system for measurement of the underwater radiance distribution," Opt. Eng. **28**, 241–247 (1989).
7. K. J. Voss, and A. L. Chapin, "Upwelling radiance distribution camera system, NURADS," Opt. Express **13**(11), 4250–4262 (2005).
8. K. J. Voss, "Use of the radiance distribution to measure the optical absorption coefficient in the ocean," Limnol. Oceanogr. **34**(8), 1614–1622 (1989).
9. K. J. Voss, A. Morel, and D. Antoine, "Detailed validation of the bidirectional effect in various Case 1 waters for application to ocean color imagery," Biogeosciences **4**(5), 781–789 (2007).
10. C. F. Bohren, and D. R. Huffman, *Absorption and Scattering of Light by Small Particles* (John Wiley and Sons, New York, NY, 1983).
11. G. W. Kattawar, "Polarization of light in the Ocean," in *Ocean Optics*, R. W. Spinrad, K. L. Carder, and M. J. Perry, eds., (Oxford University Press, New York, NY. 1994).
12. J. S. Tyo, D. L. Goldstein, D. B. Chenault, and J. A. Shaw, "Review of passive imaging polarimetry for remote sensing applications," Appl. Opt. **45**(22), 5453–5469 (2006).
13. L. B. Wollf, and A. G. Andreau, "Polarization camera sensors," Image Vis. Comput. **13**(6), 497–510 (1995).
14. C. J. Zappa, M. L. Banner, H. Schultz, A. Corrada-Emmanuel, L. B. Wolff, and J. Yalcin, "Retrieval of short ocean wave slope using polarimetric imaging," Meas. Sci. Technol. **19**(5), 055503 (2008).
15. K. J. Voss, and Y. Liu, "Polarized radiance distribution measurements of skylight. I. System description and characterization," Appl. Opt. **36**(24), 6083–6094 (1997).
16. J. L. Pezzaniti, and D. B. Chenault, "A division of aperture MWIR imaging polarimeter," Proc. SPIE **5888**, 58880V (2005).
17. C. K. Harnett, and H. G. Craighead, "Liquid-crystal micropolarizer array for polarization-difference imaging," Appl. Opt. **41**(7), 1291–1296 (2002).
18. G. Horváth, A. Barta, J. Gál, B. Suhai, and O. Haiman, "Ground-based full-sky imaging polarimetry of rapidly changing skies and its use for polarimetric cloud detection," Appl. Opt. **41**(3), 543–559 (2002).

#130976 - $15.00 USD Received 30 Jun 2010; revised 24 Aug 2010; accepted 25 Aug 2010; published 31 Aug 2010

19. H. Schenck, Jr., "On the focusing of sunlight by ocean waves," J. Opt. Soc. Am. **47**(7), 653–657 (1957).
20. J. R. V. Zaneveld, E. Boss, and A. Barnard, "Influence of surface waves on measured and modeled irradiance profiles," Appl. Opt. **40**(9), 1442–1449 (2001)..
21. Y. You, D. Stramski, M. Darecki, and G. W. Kattawar, "Modeling of wave-induced irradiance fluctuations at near-surface depths in the ocean: a comparison with measurements," Appl. Opt. **49**(6), 1041–1053 (2010).
22. T. W. Cronin, and N. Shashar, "The linearly polarized light field in clear, tropical marine waters: spatial and temporal variation of light intensity, degree of polarization and e-vector angle," J. Exp. Biol. **204**(Pt 14), 2461–2467 (2001).
23. B. Lundgren, "*On the polarization of the daylight in the sea*," (Copenhagen University, Copenhagen, Denmark **17**, 34 (1971).
24. A. Tonizzo, J. Zhou, A. Gilerson, M. S. Twardowski, D. J. Gray, R. A. Arnone, B. M. Gross, F. Moshary, and S. A. Ahmed, "Polarized light in coastal waters: hyperspectral and multiangular analysis," Opt. Express **17**(7), 5666–5683 (2009).
25. J. S. Tyo, "Optimum linear combination strategy for an N-channel polarization sensitive imaging or vision system," J. Opt. Soc. Am. A **15**(2), 359–366 (1998).
26. K. J. Voss, and G. Zibordi, "Radiometric and geometric calibration of a spectral electro-optic "fisheye' camera radiance distribution system," J. Atmos. Ocean. Technol. **6**(4), 652–662 (1989).
27. K. J. Voss, and E. S. Fry, "Measurement of the Mueller matrix for ocean water," Appl. Opt. **23**(23), 4427–4439 (1984).

1. Introduction

The in-water and water-leaving radiance in the ocean is partially polarized and this has implications for both biological activity [1] and for viewing the ocean from a satellite. The biological implications of the polarization are a current topic of research [2], but the implications for ocean color remote sensing are just being exploited [3,4]. Besides using the polarization of the water leaving radiance for studies of the water properties, this polarization may be important for ocean color sensors which have unintended polarization sensitivities [5].

Measurements of the scalar (without regard to polarization) in-water spectral upwelling radiance distribution have occurred more frequently since the development of RADS [6] and then NuRADS [7]. These instruments use electro-optic camera systems combined with filter-changers and fisheye cameras to image the complete upwelling radiance distribution, for a specific wavelength, in one image. The CCD resolution and optics allow measurement of the radiance distribution with 1° angular resolution. These systems have been used in studies looking at the in-water light field [8] and tests of the angular radiance distribution variations in ocean color algorithms [9].

The light field polarization is easily described by use of the four parameter Stokes Vector, which has been defined many times, for example in Bohren and Huffman [10] and Kattawar [11]. These four parameters are prescribed relative to some reference plane, in our case we will choose the plane defined by the viewing direction and the nadir direction. With this plane, E_L is the component of the electric field in the plane, E_R is the component perpendicular to this plane, with the sense that E_L x E_R is along the direction of propagation. With these definitions, the electric field can be written as:

$$E_L = E_{ox} \exp\left[i\left(\omega t + \delta_x\right)\right] \tag{1}$$

$$E_R = E_{oy} \exp\left[i\left(\omega t + \delta_y\right)\right], \tag{2}$$

where ω is the frequency of the electric field, δ_x and δ_y are a relative phase factor, and E_{ox} and E_{oy} are the amplitude of the electric field in the plane and perpendicular to the reference plane, respectively. With these definitions the Stokes parameters are defined as:

$$I = E_L E_L^* + E_R E_R^* = {E_{ox}}^2 + {E_{oy}}^2 \tag{3}$$

$$Q = E_L E_L^* - E_R E_R^* = {E_{ox}}^2 - {E_{oy}}^2 \tag{4}$$

$$U = E_L E_R^* + E_R E_L^* = 2E_{ox}\ \ E_{oy}\ \cos\delta \tag{5}$$

#130976 - $15.00 USD Received 30 Jun 2010; revised 24 Aug 2010; accepted 25 Aug 2010; published 31 Aug 2010

$$V = E_L E_R^* + E_R E_L^* = 2E_{ox} \quad E_{oy} \ \sin\delta \tag{6}$$

$$\delta = \delta_y - \delta_x \tag{7}$$

Where (*) represents the complex conjugate, and δ is the relative phase shift between the E_L and E_R.

Techniques to find the polarization of the light field have been reviewed in Tyo et. al. [12] and Wolff and Andreau [13]. The various techniques can be thought of as Division of Amplitude (e.g. Zappa et al. [14]), Division of Time (DOT, e.g. Voss and Liu [15]), Division of Aperture (e.g. Pezzaniti and Chenault [16]), Division of focal plane (e.g. Harnett and Craighead [17]) and co-boresighted (e.g. Horvath et al. [18]). For clear sky atmospheric measurements the simplest measurement technique is DOT [15] but many of the other techniques have been used.

In the water, the light field is constantly changing due to the interaction of the incident light field with surface waves [19–21]. Thus a DOT technique is not applicable. In-water measurements have predominately been done with 3 or 4 boresighted radiometers, to obtain the Stokes vector in a single direction, then either manually [22] or mechanically [23] moved into different directions. One advantage of the single direction radiometer systems is that hyperspectral data can be obtained [24]. With a fisheye camera radiometer, the complete hemisphere of radiance information can be obtained for a given wavelength, and thus by boresighting three of these fisheye systems we can measure the dynamic polarized upwelling light field, as was done with more rapidly changing (cloud) atmospheric measurements [18]. In this paper we will have a short description of this instrumentation, as it is small change from our basic NuRADS system, describe the polarization steps required beyond the normal radiometric calibration, then give an example of the data collected with this system.

2. PolRADS instrument description

PolRADS is fundamentally based around three NuRADS systems [7]. Each NuRADS system has a fisheye lens, relay optics, a 6 wavelength filter changer, and a CCD camera (Apogee AP260EP). We also have a computer and hard drive in each NuRADS housing to control the camera and store the data. In the field, communication with the onboard computer is established via Ethernet connection supplied with surface power through an umbilical cable. Each system also has an electronic compass/tilt-roll device, however because this device was too slow, images were navigated by looking at the anti-solar position that was obvious in the radiance data. For the PolRADS configuration the NuRADS systems were modified in two ways. First, the plastic dome windows in the system were replaced by glass dome windows. Plastic windows can have stress bi-refringence that would affect the polarization of the light incident on the system in a manner that could not be characterized. Second, a linear polarizer is placed in the optical path and used as a polarization analyzer. The NuRADS were then fixed in a triangular arrangement, such that the linear polarizers are oriented at an angle of 0°, 60° and 120° (± 5°). Three polarizer positions are required to determine the intensity and the two linear polarization Stokes parameters, and these angles provide one optimal set of orthogonal measurements [25]. Fig. 1 shows the POLRADS assembly. The spectral response of the system is determined by the interference filters placed in the filter changer. We used 6 filters, nominally 10 nm bandwidth, spread through the visible region but emphasizing the transmission bandpass of the water (filters were at 410, 436, 486, 526, 548, and 616 nm).

3. Characterization and calibration

The radiometric steps for calibrating a scalar fisheye camera system have been described previously [7,26] and must be done for each camera system independently. These steps consist of the angular, roll off, linearity, and immersion calibrations for each system.

The basic equations describing the derivation of the Stokes parameters, I, Q, and U, from the camera system can be described by the following matrix equation.

#130976 - $15.00 USD Received 30 Jun 2010; revised 24 Aug 2010; accepted 25 Aug 2010; published 31 Aug 2010

$$\begin{bmatrix} I \\ Q \\ U \end{bmatrix} = \begin{bmatrix} a & b & c \\ d & e & f \\ g & h & i \end{bmatrix} \begin{bmatrix} S1 \\ S2 \\ S3 \end{bmatrix} \tag{8}$$

In this equation *S1*, *S2*, and *S3* are the camera counts obtained from each camera system for the same point in the radiance distribution (same nadir angle, θ, and azimuth angle, ϕ). *I, Q*, and *U* are the Stokes parameters for those angles, and *a-i* are the elements of a transformation matrix that relates the camera counts to the Stokes vector. *S1*, *S2*, and *S3* have to be corrected, before this stage for characterization/calibration factors specific to the individual cameras such as the lens rolloff and immersion factor. The angular calibration for each camera is used to obtain the correct position in the radiance distribution from the pixel location on the specific camera image plane.

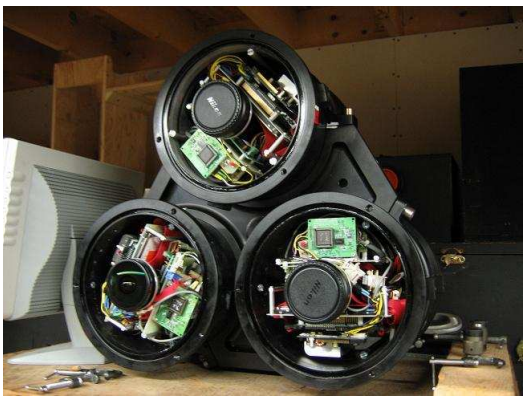

Fig. 1. Polrads assembly with three NuRADS cameras in a triangular arrangement. Shown without the cover plates, and glass dome windows.

So the central problem in obtaining the Stokes vector is to find the proper transformation matrix. To do the polarization calibration we place the camera assembly in front of the exit port of a 1-meter integrating sphere. This integrating sphere provides a uniform radiance source with no polarization. A linear polarizer sheet is then placed between the POLRADS instrument and the exit port of the sphere. The polarizer sheet is mounted in a rotation holder, so that the relative orientation of the polarizer can be determined very accurately (< ± 1°). We then rotate this polarization sheet from 0°-180° in 10° steps, acquiring an image with each camera at each step. An average of a 4 x 4 pixel area in the center of the image of the exit port was abstracted from each of the images. This results in a set of 19 equations where we know I_ψ, Q_ψ, U_ψ and $S1_\psi$, $S2_\psi$, and $S3_\psi$, the values of the Stokes vectors and the camera intensities for each polarizer angle, ψ. At this stage we assume that I_ψ, Q_ψ, and U_ψ are given by:

$$I_\psi = 1 \tag{9}$$

$$Q_\psi = \cos(2\psi + \Delta) \tag{10}$$

$$U_\psi = \sin(2\psi + \Delta) \tag{11}$$

Where Δ is an arbitrary offset angle for the polarizer. This is simply *I*, *Q*, and *U* for a fully linearly polarized light beam, with a plane of polarization given by ψ.[11] We then perform a non-linear fit of the equations:

$$I_\psi = a\ S1_\psi + b\ S2_\psi + c\ S3_\psi \tag{12}$$

$$Q_\psi = d\ S1_\psi + e\ S2_\psi + f\ S3_\psi \tag{13}$$

#130976 - $15.00 USD Received 30 Jun 2010; revised 24 Aug 2010; accepted 25 Aug 2010; published 31 Aug 2010

$$U_{\psi} = g\ S1_{\psi} + h\ S2_{\psi} + i\ S3_{\psi} \tag{14}$$

to determine *a*-*i*, the transformation matrix. This process is repeated for each camera channel, resulting in a transformation matrix for each system channel or wavelength.

Once the transformation matrix is determined, the absolute calibration can be done. The above analysis presumes that *I* is unity, thus the transformation matrix obtained is actually normalized to the sphere radiance at that particular channel. The absolute calibration is done in a similar manner to the scalar, non-polarized, systems (with an FEL standard lamp and a reflectance plaque), but in this case images of the reflectance plaque with the POLRADS system were obtained then the transformation matrix, listed above, was applied to find a relative value of *I*, *Q/I* and *U/I*. Knowing the reflectance of the plaque and the irradiance of the lamp we can predict the radiance that the system is viewing, and a calibration factor, K_{λ}, relating this radiance with the derived *I* can be calculated. The transformation matrix for each channel (wavelength) can then be multiplied by this K_{λ} to obtain the overall matrix that gives *I, Q*, and *U* in engineering units ($\mu W\ cm^{-2}\ nm^{-1}\ sr^{-1}$).

4. Uncertainty in polarization retrievals

The uncertainty in this polarization retrieval comes from several sources. The first is an uncertainty in the characterization of each individual camera system. The second would be a pointing error, or misalignment of the three systems, which causes data, which does not represent the same direction, to be combined. The third source would be errors due to the shutter exposure accuracy in each system. Lastly there is the uncertainty in the determination of the transformation matrix.

For the first factor, since the polarization calibration is done with the system looking straight into the integrating sphere, there is an uncertainty introduced through the rolloff calibration between the cameras at angles off of nadir. The normalized rolloff factor is shown below in Fig. 2 for the three cameras. We estimate that our rolloff calibration is accurate for these systems to within ± 2% based on how well our equation characterizing the rolloff fit the calibration data. To see the effect on the retrieved Stokes vectors we took the results from a pixel in each camera image, then added a small (different) offset due to this error to each of the three pixel values. This process was done 10,000 times, each time picking an offset so that the standard deviation of the offsets was 2%. We found that the 2% error in rolloff calibration resulted in an approximately 2% error in *I*, *Q*, and *U*. Doing the process 100,000 times changed the result insignificantly (0.1% or less).

#130976 - $15.00 USD Received 30 Jun 2010; revised 24 Aug 2010; accepted 25 Aug 2010; published 31 Aug 2010

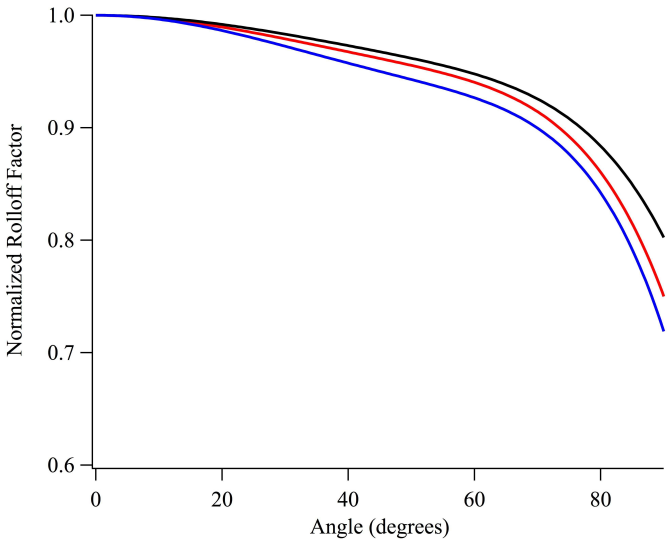

Fig. 2. Normalized rolloff for the three cameras. The rolloff correction is less than 10% at angles less than 75°.

For the second factor, we estimate the error in bore-sighting the cameras, then retrieving correlated pixels to be ± 1°. Fortunately, in the upwelling radiance distribution the light field is fairly uniform, and the polarization features change slowly. To estimate the error in this we once again did a similar process to that described above; we did 10,000 inversions to obtain *I*, *Q*, and *U*, where for each inversion the data point pulled out of the each image was offset by a small amount (the standard deviation of the offset was 1°). With this we found that the percent standard deviation in the retrieved *I*, *Q*, and *U* was on the order of 2%, however this error grew to 3% towards the edge of the image, where the upwelling radiance distribution was changing more rapidly.

The next source of error would be the errors due to shutter exposure accuracy between the cameras. These exposures are relatively long (on the order of 0.5 s) and these errors are on the order of a millisecond or less, so the error is relatively small, significantly less than 2%. This propagates through to *I*, *Q*, and *U* and causes an error on the order of 2%, similar to the rolloff calibration error.

Lastly there is the error in the determination of the transformation matrix. We tried to estimate this error by repeating the polarization calibration, obtaining a new data set with linearly polarized light entering the system, to get an independent set of polarization data. This data was then processed with the transformation matrix. We found no systematic difference between the predicted and retrieved *I*, *Q*, and *U*; however there seemed to be a standard deviation of the difference on the order of 2%. Including this may be overcounting, as it probably includes the shutter exposure error to some extent, but we include this as a possible additional source of error.

Other possible error sources could be mismatch between spectral filtering on each system, mistiming of the synchronization of each camera, and the ever present self-shadowing of the water column by the instrument itself. The spectral filter in each camera came from a matched set, so while there were probably small differences between these filters, the difference in the center band of the filters was less than 1 nm. This is probably a negligible factor over much of the spectrum, but depends on the water properties so care should be taken. The synchronization between the cameras was done with a separate electronic signal, generated by an electronic pulse to the camera, so the images were synchronized within 10 ms, which with a 0.5 s exposure makes this factor negligible for the upwelling light field.

The final issue, self-shadowing, is always an issue in passive ocean optics instrumentation, particularly when looking at upwelling light. This may be a bigger problem in this instrument

#130976 - $15.00 USD Received 30 Jun 2010; revised 24 Aug 2010; accepted 25 Aug 2010; published 31 Aug 2010

because the shadowing will change slightly between the different cameras, due to their slightly different position in the overall shadow. It would be very difficult to predict and offset this error, due to the non-symmetric aspect of the final instrument and its dependence on the sun/instrument orientation. The main point is to be careful when looking at data near the anti-solar point or in more turbid water where absorption is higher.

Adding the different error sources in quadrature results in an estimate of the total uncertainty of 5% to 6% in *Q*, and *U* (and Degree of Linear Polarization, *DOLP*). We have not detailed the possible errors in the absolute value of *I*, which include uncertainties in the absolute radiance calibration. This includes uncertainties in the lamp irradiance, laboratory setup, and spectralon plaque reflectance and is estimated to be on the order of 5%, so the uncertainty of the absolute radiance, *I*, would be on the order of 7-10%.

5. Sample data

As an example data set we show a PolRADS data product acquired in clear water off of Hawaii in 2005 (Chlorophyll concentration was approximately 0.1 mg/m^3). These images were all acquired at a depth of 0.3 m. Typically data is taken continuously while the instrument is deployed. Since a full cycle of data at each wavelength takes approximately 2 minutes, typically 5 images are obtained at each wavelength in a 10-minute period. In this example, the data product shown is the average of 3 images acquired on December 2, 2005, off of Lanai Hawaii (20.83° N, 157.18° W) at 526 nm, taken in a 6 minute period around 22:00 UTC. The solar zenith angle was 43°. Since the radiance distribution should be symmetric around the principal plane, the left and right side of the principal plane in each image were averaged together, thus the resultant image is an average of 6 hemispheres of data. This averaging helps to reduce the effects of wave focusing in the images. Figure 3 shows *I*, *Q/I* and *U/I*. These images are in a fisheye projection, where the edge of the image is at 88° from nadir, and nadir angle is proportional to the distance from the center. Figure 3A is the radiance in units of $\mu W\ cm^{-2}\ nm^{-1}\ sr^{-1}$. The minimum radiance is on the solar side of the radiance distribution, at a scattering angle of approximately 90° from the direct solar beam. There is another minimum slightly above the anti-solar position, where the instrument self shadowing occurs.

Figure 3B shows *Q/I* (on left) and *U/I* (on right). *Q/I* is symmetric across the principal plane, and has a minimum in the direction towards the sun, at the 90° scattering angle. It is near zero in the backscattering direction, reflecting the effect of the unpolarized incident solar beam and the ocean Mueller matrix.[27] *U/I* is near zero along the principal plane, but reaches a maximum towards the horizon, but at an azimuth near 45° from the solar direction. Most of this pattern can be described by a single scattering approximation and the ocean Mueller matrix, but there is some modification due to multiple scattering, a topic to be discussed in a later paper.

Figure 4 shows the percent standard deviation for the imagers shown above. Due to wave focusing and other variations in the lightfield between the data images, this ranges up to 10%. The wave focusing shows up as the stripes emanating from the anti-solar point. The anti-solar point shows as a maximum in the percent standard deviation, partly because it is a minimum in the radiance. Similarly, the regions of high percent standard deviations in *Q/I* and *U/I* occur where *Q/I* and *U/I* are relatively small.

The *DOLP* of the incoming light as well as the angle of polarization were computed using the Stokes vector and are shown in Fig. 5. The *DOLP* is greater than 60% in these clear water and sky conditions. The minimum in *DOLP* occurs in the anti-solar direction, while the maximum occurs around the 90° scattering direction from the direct solar beam. The plane of polarization is typically near 90° to the scattering plane (containing the direct solar beam and the observation direction). The geometry of this image is related to the interplay between this and the reference system used in these images.

#130976 - $15.00 USD Received 30 Jun 2010; revised 24 Aug 2010; accepted 25 Aug 2010; published 31 Aug 2010

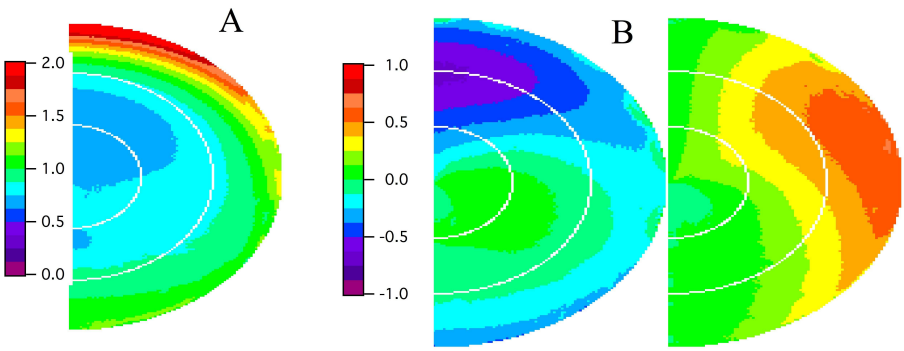

Fig. 3. Radiance, *I*, (A), *Q*/*I* and *U*/I (B). Fisheye projection such that sun is towards the upper part of the figure, nadir angle is proportional to distance from center with center of each hemisphere representing the nadir direction. Units for Radiance are μW cm^{-2} nm^{-1} sr^{-1}, while *Q*/*I* and *U*/*I* range are normalized and range from −1 to 1. Data is at 526 nm. White lines are at 30° and 60° nadir angle.

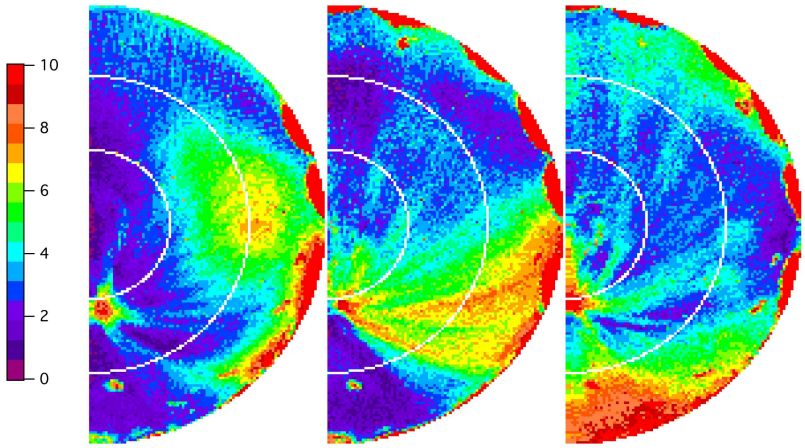

Fig. 4. Calculated percent standard deviation in I, Q/I and U/I shown in Fig. 3. White lines are at 30° and 60° nadir angle.

6. Conclusions

We have developed a new system to measure the polarized upwelling radiance distribution. This system measures the Stokes parameters *Q*/*I* and *U*/*I* with a 0.05-0.06 uncertainty and *I* with a 7-10% uncertainty. The example measurement shown, from clear water and skies, shows that the upwelling radiance can be highly polarized (>60%), depending on view angle. Data from this instrument will be used to compare with results from radiative transfer models of the polarized upwelling radiance distribution. With these results, corrections for the polarization of the upwelling radiance field in satellite ocean color sensors can be developed and the use of polarization to obtain additional information from the remote sensing signal can be investigated.

#130976 - $15.00 USD Received 30 Jun 2010; revised 24 Aug 2010; accepted 25 Aug 2010; published 31 Aug 2010

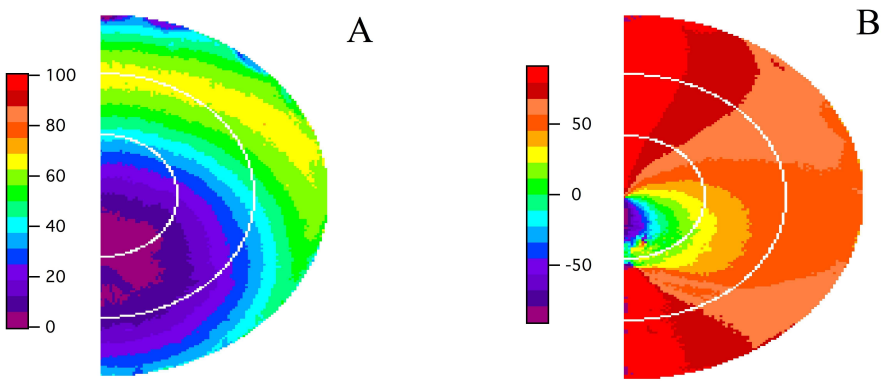

Fig. 5. Percent *DOLP* (A) and plane of polarization (B). Maximum DOLP is >60%. White lines are at 30° and 60° nadir angle.

Acknowledgement

This work was supported by NASA (contract numbers NNG04HZ21C and NNX08AH93A). The Ocean Optics program at ONR has also supported the development of our radiance distribution camera systems. The data shown was collected on a NASA/NOAA supported cruise.

#130976 - $15.00 USD Received 30 Jun 2010; revised 24 Aug 2010; accepted 25 Aug 2010; published 31 Aug 2010